AIAA JOURNAL
Vol. 34, No. 3, March 1996

Simultaneous Water Vapor Concentration and Temperature Measurements Using 1.31-μm Diode Lasers

Mark G. Allen* and William J. Kessler†
Physical Sciences, Inc., Andover, Massachusetts 01810

This paper reports the development of a compact, inexpensive sensor for simultaneous water vapor concentration and temperature measurements suitable for aeropropulsion exhaust applications. High sensitivity is achieved with an electronically balanced dual detector strategy that circumvents requirements for custom-fabricated lasers operating at specific wavelengths or high-frequency modulation techniques. Using widely available, broadly tunable InGaAsP diode lasers near 1.31 μm, simultaneous measurements are demonstrated in a fiber-coupled, wavelength multiplexed configuration with a limiting density sensitivity of 10^{15} cm^{-3} in a 50-cm path and an rms standard deviation of 42 K over a range from 300 to 1300 K. Initial results suggest the possibility of extending this temperature range to 1900 K and above using other line pairs.

I. Introduction

COMPACT, lightweight, and rugged sensors for in-stream measurements of aeropropulsion flow parameters and desired for improved testing, engine health or emissions monitoring, and control applications. In addition to the fundamental gasdynamic properties, such as density, chemical composition, temperature, velocity, and pressure, simultaneous multiproperty measurements are desired for higher order parameters, such as mass flux ρV and thrust ρV^2. Significant work during the past decade has demonstrated in-situ techniques for all of these property measurements based on laser-induced fluorescence, Rayleigh scattering, and various coherent laser scattering approaches. These techniques, however, generally require large and complex multiple laser sources that are incompatible with widespread field or flight applications.

Recently, however, spectroscopic-grade, room-temperature tunable diode laser sources have become available in a number of wavelength regions between about 630 nm and 2.1 μm. Many of the laser sources are engineered for remote installation, high bandwidth communications applications and are characterized by continuously declining price/performance ratios, improved lifetime and stability, and compatibility with fiber-optic distribution networks. Their application to absorption measurements in atmospheric and environmental monitoring is relatively mature, and commercial units are now available for industrial applications.

As demonstrated in Refs. 1–5 diode laser-based absorption techniques can be used to obtain path-averaged measurements of all of the gasdynamic parameters mentioned, as well as multiparameter combinations such as mass flux and thrust. Most aeropropulsion-related techniques demonstrated to data involve absorption measurements on overtone and combination bands of H_2O between 1.3 and 1.4 μm or the ($b \leftarrow X$) electronic system of O_2 near 763 nm. In this paper, we describe recent progress toward the development of a field- and flightworthy sensor for simultaneous water vapor density and temperature measurements. High sensitivity is obtained using an electronically balanced dual-beam technique that offers several potential advantages for practical devices compared to more traditional frequency-modulation or custom-fabricated laser approaches.[6–8]

II. Absorption Spectroscopy for Aerodynamic Parameters

All of the diode laser sensor configurations and based on absorption of the wavelength-tuned laser intensity as the beam propagates across the measurement path. This absorption is described by the Beer-Lambert relation

$$I_\nu = I_{\nu,0} \exp[S_{(T)} g(\nu - \nu_0) N \ell] \tag{1}$$

where I_ν is the monochromatic laser intensity at frequency ν, measured after propagating a pathlength ℓ through a medium with an absorbing species number density N. The strength of the absorption is determined by the temperature-dependent line strength $S_{(T)}$, and the line shape function $g(\nu - \nu_0)$. The line shape function describes the temperature- and pressure-dependent broadening mechanism of the fundamental line strength. The temperature dependence of the line strength arises from the Boltzmann population statistics governing the internal energy level population distribution of the absorbing species.

The single-mode distributed feedback (DFB) diode lasers used in this work are sufficiently narrow in frequency that they may be considered essentially monochromatic with respect to the absorption line shape. The laser frequency may be tuned over a range that encompasses the entire line shape function so that the resultant transmission can be integrated to remove the pressure and temperature dependence of the line-broadening mechanisms. The recorded absorbance, then, is proportional only to the temperature-dependent line strength and the absorbing species number density. It is usually possible to select an absorbing ground state whose line strength is relatively constant over some target temperature range so that the absorbance is a direct measurement of species number density. Separate temperature measurements may be used to correct for temperature variations, if necessary.

Alternatively, two absorption transitions may be probed (using one or two lasers, depending on the target transition separation and the laser tuning range). The ratio of the integrated absorbance of each transition is a pure function of temperature,[2]

$$R = \left(\frac{S_1}{S_2}\right)_{T_0} \cdot \exp\left[-\frac{hc\Delta E}{k}\left(\frac{1}{T} - \frac{1}{T_0}\right)\right] \tag{2}$$

where S_1 and S_2 are the line strength values at some reference temperature T_0, and ΔE is the energy separation of the absorbing states expressed in wave number units (reciprocal centimeters). The temperature sensitivity depends on the values of the reference line strengths and the energy separation, as will be discussed in more detail subsequently. With the temperature so determined, either or both absorbances can be used to determine the number density.

III. Sensor Architecture

High-performance near-IR diode lasers are widely available in two narrow spectral windows near 1.31 and 1.55 μm. For water vapor measurements, custom fabricated InGaAsP diode lasers are

Received Feb. 1, 1995; revision received May 25, 1995; accepted for publication June 9, 1995.

*Principal Research Scientist, 20 New England Business Center.
†Principal Scientist, 20 New England Business Center.

available near 1.39 μm, corresponding to combination-band transitions with typical line strengths on the order of 10^{-21} cm/mol, resulting in atmospheric absorbances of a few percent per centimeter of pathlength. Near 1.31 μm, the wavelength corresponding to minimum dispersion of fiber optic networks, devices manufactured for high bandwidth CATV applications are available from a number of vendors. Laser diodes generating in excess of 10 mW are available for under $4000 in optically isolated pigtail packages that can be continuously injection-current tuned over 2.5 cm^{-1}. In this wavelength region, a mixture of $2\nu_3$ and $\nu_1 + \nu_3$ water transitions are available, although peak line strengths are at least a factor of 100 weaker than the transitions near 1.39 μm.

For measurement of weak absorbances below about 10^{-3}, special techniques must be applied to overcome excess laser amplitude noise. The most common of these techniques imposes of modulation on the diode laser injection current that, in turn, generates an amplitude and frequency modulation on the laser intensity. The absorbance is detected at the modulation frequency, or some harmonic, using bandpass filtered, phase-sensitive techniques to reject the out-of-band laser amplitude noise. Depending on the depth and frequency of the injection current modulation, this general technique is known as frequency or wavelength modulation spectroscopy (hereafter both techniques will be referred to as FM spectroscopy).[9] Using these techniques, absorbances as low as a few parts in 10^7 have been achieved in a 1-Hz bandwidth, and instruments based on FM spectroscopy have been fielded in numerous atmospheric monitoring applications over the last decade.

FM techniques, however, have several potential disadvantages for some practical applications. Optimum sensitivity is achieved with modulation bandwidths comparable to the absorption half-widths, which implies GHz bandwidths for atmospheric-pressure measurements. Lower frequency variants of wavelength modulation spectroscopy reduce this requirements to megahertz levels,[1] but still require rf-electronics and phase-sensitive amplifiers. With higher modulation frequencies, the frequency range over which the laser center frequency may be scanned is reduced. The magnitude of this reduction is highly device dependent, but factors 2–10 have been observed on O_2 and H_2O measurements.[10,11] This constriction may inhibit the laser's ability to fully scan a pressure-broadened line shape, thereby complicating baseline subtraction procedures and introducing pressure and temperature dependencies in the measured absorbance due to line shape variations. Furthermore, the additional rf components add to the cost and weight of a stand-alone sensor system.

The approach for sensitive absorption measurements pursued in the present water vapor sensor is based on a dual-beam technique with electronic balancing originally developed by Hobbs[12] at IBM for communications applications and used to demonstrate shoot-noise-limited absorption measurements of I_2 vapor.[13] In principle, dual-beam approaches that divide the signal beam intensity (passing through the absorbing medium) by a reference beam intensity (not passing through the absorbing medium) should allow cancellation of common-mode excess laser amplitude noise. In practice, however, conventional dual-beam measurements are severely limited by the balancing requirements in the two detection channels.[14] For example, if the target detectivity in 10^{-6} and the laser amplitude noise in the detection bandwidth is 1% of the mean intensity, then the laser intensity incident on the two detectors must be balanced to less than 1 part in 10^4. Even if this balance could be achieved in a laboratory setup, it would be impractical to maintain in a field instrument. Furthermore, spatial variations in detector responsivity, drifts in amplifier or other circuit characteristics, changing intensities in the two beams due to polarization or reflectance variations during a laser scan, and a lack of high-bandwidth phase coherence in transimpedance amplifiers all contribute to additional noise on the voltage ratio.

The measurements reported here were all obtained using an electronic balancing technique that circumvents these limitations. A schematic of the basic circuit fragment developed by Hobbs is shown in Fig. 1 (taken from Ref. 13). The essential innovation of the balanced ratiometric detector (BRD) is to replace optical balancing of a conventional dual-beam detection system with electronic

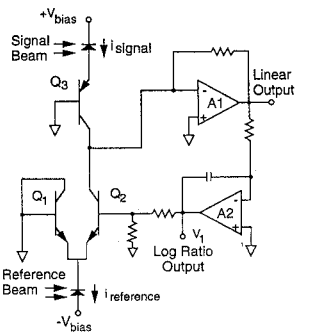

Fig. 1 Schematic of basic components of balanced ratiometric detector (from Ref. 13).

cancellation of the photodetector currents. Since InGaAs photodetectors exhibit wide dynamic range linearity, coherent photocurrent balancing is possible over the entire frequency band within which typical diode lasers exhibit significant noise power. Noise cancellation is achieved by balancing the photocurrents at the summing junction of amplifier A_1 so that its output is nulled. By arranging the reference beam photocurrent to exceed the signal beam photocurrent and splitting the reference beam photocurrent across the differential bipolar junction transistors Q_1 and Q_2, the currents at the summing junction can be balanced by adjusting the base-emitter voltage of the transistor pair, providing an electronic photocurrent balance as opposed to an optical intensity balance. The balance is maintained through a feedback loop from the integrating amplifier A_2.

The output of the integrating amplifier is given by

$$V_1 = G \log[(I_{ref}/I_{sig}) - 1] \tag{3}$$

where G is the fixed gain of the integrating amplifier. Substituting Eq. (1) for the ratio I_{ref}/I_{sig}, we derive the relationship between the measured voltage and laser absorbance α_ν,

$$V_1 = G \log[B \exp(\alpha_\nu) - 1] \tag{4}$$

where α_ν is defined as

$$\alpha_\nu \equiv S_{(T)} g_{(\nu-\nu_0)} N \ell \tag{5}$$

and B is the baseline ratio of I_{ref}/I_{sig} in the absence of an absorber. For small absorbances, this feedback voltage is linearly proportional to the absorbance with a constant of proportionality determined by the baseline ratio and amplifier gain. Recording the voltage as the laser frequency is scanned across an absorption line shape provides a direct measure of the transition line strength that can be absolutely related to the absorber number density provided that the baseline ratio is known.

We have assembled several versions of this basic circuit fragment, including additional amplifiers and circuitry to separately determine calibration signals. We have used both Si and InGaAs detectors with equal sensitivity. For practical aeropropulsion applications, this approach has the advantage that the circuitry may be assembled on a single printed circuit board. Present models are fabricated using low-noise assembly techniques into separate enclosures measuring about 5 × 2 × 10 cm and the output is available for digitization, additional amplification, or direct oscilloscope display. Absorbance signals of 10^{-5} are usually observable in a single sweep on an oscilloscope trace.

Fiber-coupled sensor configurations are often desirable for field or flight systems and are used in the water vapor measurements reported here. They permit easy optical alignment, interference-free beam transport, and remote siting to laser sources and detectors. At 1.31 μm, single-longitudinal mode DFB lasers are available from many vendors in isolated pigtail packages. In these devices, the diode laser, a monitor photodetector, and thermoelectric cooler/heater are preassembled into a dual-inline or butterfly type circuit package. The output from the diode laser is collimated using antireflection coated optics and directed through a monolithic Faraday isolator, after which it is recoupled into a single-mode fiber. The collimating optics and isolator are precision aligned by the manufacturer in an

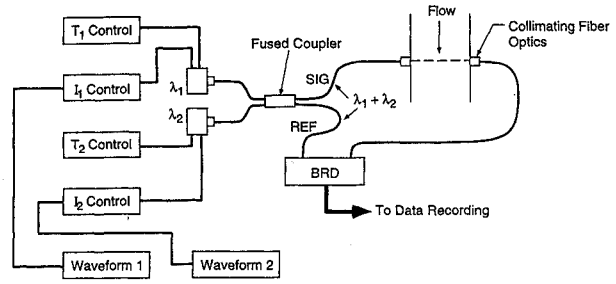

Fig. 2 Layout of dual-laser water vapor concentration and temperature sensor.

enclosed, laser-welded assembly known as a pigtail. The optical isolator is a critical element in ultrasensitive absorption-based sensors. The small gain volume and low threshold intensity of diode lasers makes them particularly sensitive to low levels of back-reflected light from optical surfaces in the fiber distribution network. Back reflections of −40 dB are sufficient to induce frequency and amplitude oscillations in the laser or to drive additional modes above threshold.

Figure 2 shows the arrangement of the dual-laser water vapor concentration and temperature measurement system. Two fiber pigtailed InGaAsP diode lasers (Mitsubishi FU-45SDF-38) operating near 1.31 μm are supported in separate temperature-stabilized mounts. The fiber pigtails are connected to a wavelength-flattened, single-mode 2 × 2 fiber coupler (Gould Electronics) that couples 50% of the intensity from each laser into each of the output fibers. One fiber carries the signal channel to the measurement location, where antireflection coated optics (Oz Optics) collimate the fiber output into a 1-mm-diam beam. This beam is recaptured by a matched set of optics and returned to the signal channel photodetector of the BRD. The second fiber carries the reference channel directly to the BRD.

The temperature of each laser is controlled using an ILX model LDT-5910B temperature controller to adjust the laser wavelength to the center of the desired scan range. The injection current into each laser is provided by an ILX model LDX-3620 source, each separately controlled using a Hewlett–Packard programmable waveform generator to sweep the injection current. The injection current ramp results in a laser intensity and frequency ramp that is adjusted in amplitude so that the lasers sweep over the selected absorption line shapes. The programmable waveform generators are slaved together from a common trigger source and adjusted to be out of phase so that each laser sequentially scans a line shape and then remains at a constant frequency while the other laser scans. In this way, the two wavelengths are time-domain multiplexed into the same detection channel. The waveforms are typically scanned in a combined period of 1–100 ms. At these scan rates, injection current tuning up to 2.5 cm^{-1} has been verified.

Single-mode fiber transport is generally preferred in the diode laser pigtail and coupler for reliable splitting ratios and good mechanical stability. Flow-induced beam steering across the measurement path and mechanical vibrations may result in poor captured power stability or extreme alignment tolerances using single-mode fiber transport in the signal beam return fiber. We generally employ a 50- or 100-μm core diameter, multimode fiber for this portion of the sensor layout and have achieved good beam capture stability across supersonic flowfields with total pathlengths ~8 m. More details of the fiber components and connectors may be found in Ref. 8.

Although the layout in Fig. 2 shows individual laser control, waveform generator, and detector components, it is important to note that all of these components are also commercially available in printed circuit board versions, including the diode laser mount. This allows all of the components shown to be assembled in a standard 19-in.-wide rack-mountable module with the signal channel fiber optic cable as the only external element.

IV. Sensor Sensitivity Demonstrations

Figure 3 shows simulated water vapor absorption spectra near 7600 cm^{-1} (1.315 μm) at 500 K (solid line) and 2000 K (dotted line). The spectra were calculated using the HITRAN database assuming

Table 1 Summary of water vapor transitions examined

Line	Transition frequency, cm^{-1}	Lower state rational quantum numbers J	K_a	K_c	Band	Energy, cm^{-1}
1	7612.073	3	3	0	002	285
2	7605.7967	9	2	7	101	1202
3	7600.133	12	1	12	002	1558

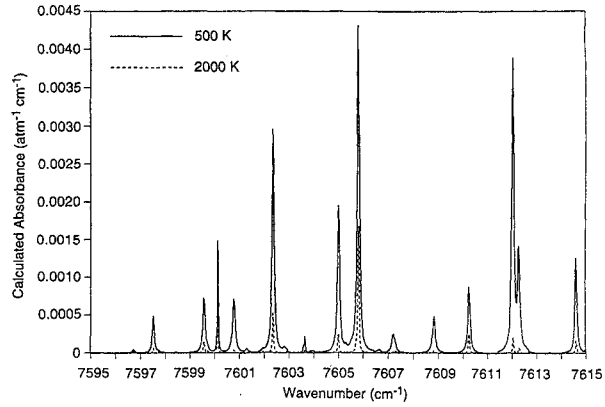

Fig. 3 HITRAN simulation of water vapor absorption near 7600 cm^{-1}.

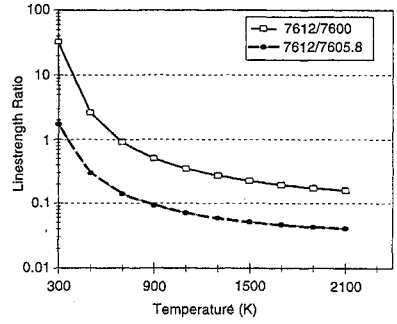

Fig. 4 Calculated line strength ratio for selected water vapor absorption pairs; calculations made using the HITRAN database with the room-temperature corrections of Toth.[16]

air broadening at 1 atm (Ref. 15). Three lines were used from this portion of the spectrum to evaluate two potential line pairs for their use in the sensor and they are summarized in Table 1. The strong low-temperature line at 7612 cm^{-1} originates from a low-energy level state with 285 cm^{-1} total energy, whereas the lines at 7605.8 and 7600 cm^{-1} originate from high-energy levels with 1202 and 1558 cm^{-1} total energy, respectively, as reported in the HITRAN database.[15] The pairs 7612/7600 and 7612/7605.8 have the largest energy level separations as tabulated by the HITRAN database for this spectral region.

Figure 4 plots the line strength ratios for the 7612/7600 pair and 7612/7605.8 pair, as calculated from the HITRAN database, corrected for the room temperature ratio by the recently published values of Toth.[16] For both pairs, the ratio falls rapidly with temperature up to about 1100 K. Above this temperature, the ratio becomes less sensitive to temperature as the population in both levels tends to decrease. The 7600 cm^{-1} transition is more than an order of magnitude weaker than the 7605.8 cm^{-1} transition at room temperature, although the exact ratio remains somewhat in question since the 7600 cm^{-1} transition is not tabulated in Toth's corrections to the HITRAN database. This larger ratio leads to an increased temperature sensitivity, as shown in Fig. 5, where we plot the absolute value of the derivative of Eq. (2) as a function of temperature for both line pairs. For a dR/dT of 10^{-4} and a target measurement uncertainty of $dR = 0.01$ (which corresponds to 10% uncertainty or less in the absorbance ratio over the range of temperatures considered), the 7612/7605.8 pair yields an uncertainty of 100 K or less at temperatures up to 900 K, whereas the 7612/7600 pair retains an uncertainty of 100 K or less to temperatures up to 1700 K.

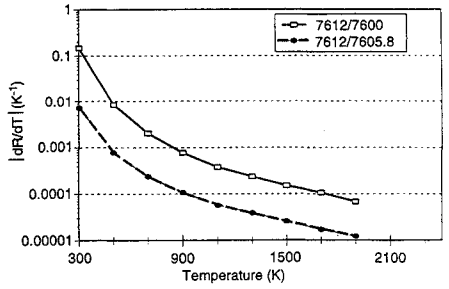

Fig. 5 Calculated temperature sensitivity, dR/dT, calculated by differentiating the results shown in Fig. 4.

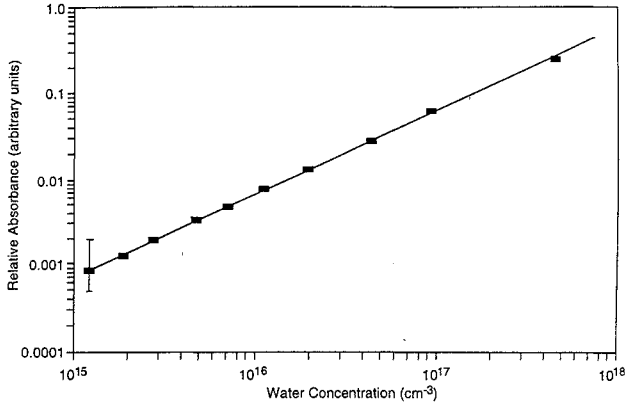

Fig. 6 Example linearity and sensitivity of water vapor concentration measurements at room temperature.

Initially, a single-laser version of the setup shown schematically in Fig. 2 was used to assess the fundamental sensitivity of water vapor density measurement in a fiber-coupled configuration. These measurements were obtained by scanning one of the diode lasers across the 7612-cm^{-1} transition and directing the beam through a room-temperature, 50-cm absorption cell fitted with antireflection coated windows. Variable concentrations of water vapor were maintained in the cell using a variable temperature water reservoir in a fixed background nitrogen pressure of 0.13 atm. Figure 6 is an example of the linearity and sensitivity of the sensor obtained with a single pass through the cell. The minimum detectable absorption signals correspond to a water vapor number density of about 10^{15} cm^{-3}, which is equivalent to an absorbance of 2×10^{-5}. The error bar in the measured absorbance at the lowest concentration is determined from the signal-to-background ratio of this measurement. The uncertainty in the data points corresponding to water concentrations greater than 10^{16} cm^{-3} is less than 5%. This minimum is determined by systematic errors in the baseline subtraction that arise from spurious etalon effects and is the typical limitation to ultrasensitive absorption measurements after the common-mode laser amplitude noise is eliminated. The uncertainty in the measured water concentration is determined by the accuracy of the temperature measurement of the water reservoir, along with capacitance manometry in the cell, and is estimated to be less than 5% over the entire range. The equivalent absorbance sensitivity is the fundamental instrumental quantity that can be used to extend these results to measurements at other temperatures and conditions. For example, using Fig. 3 as a guide and the 7605.8-cm^{-1} transition in a nominal 1-m path, the detection limit at 2000 K would be about 130 ppm.

Simultaneous temperature and density measurements were obtained in a flat flame burner and a high-temperature, variable pressure cell. The flat flame burner was a 1-in.-square Hencken-type burner operated with variable $H_2/O_2/N_2$ mixtures. Adjusting the burner stoichiometry and N_2 diluent, the gas temperature was varied from 600 to 1900 K. The measurements were made at a fixed height approximately 1 cm above the burner using a 17-pass Herriot cell configuration for a total absorption pathlength of 43 cm. The gas temperature was determined for each condition using a radiation-corrected Pt–Pt/Rh thermocouple.

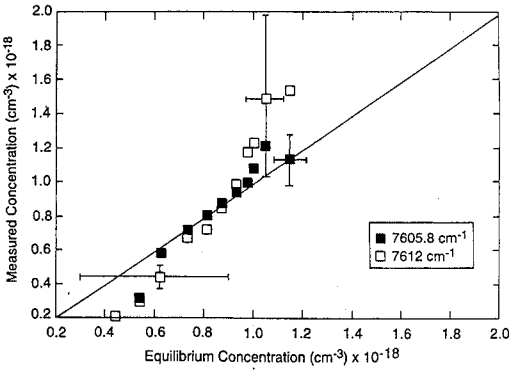

Fig. 7 Comparison of high-temperature water-concentration measurements obtained with 7612- and 7605.8-cm^{-1} transitions to equilibrium flame predictions.

For temperatures between 300 and 1300 K, a 167-cm heated quartz cell was used instead of the flat flame burner. Known water vapor and background nitrogen concentrations were introduced into the cell at room temperature. Surrounding resistive heaters were used to heat the cell over the majority of its pathlength, with approximately 15-cm total unheated pathlength at the ends of the cell near the windows. Subsequent data analysis suggested that above about 600 K the absorbance ratios were systematically perturbed by the unheated end regions of the tube, and these data were generally discarded in favor of the flame data. Temperature uniformity along the heated portion of the cell was monitored using several thermocouples, whereas variable power supplies were used to control individual heaters. The heaters and tube were enclosed in a stainless-steel pressure vessel allowing measurements at up to 5.0 atm.

Absorption measurements were acquired using the time-domain multiplexing approach already described. Each absorbance trace was averaged over typically 100 scans with a 1–10 kHz scan rate for a total measurement time on the order of 0.1–0.01 s. The raw data were corrected for baseline variations and the resulting line shape integrated to yield a quantity proportional to the integrated transition line strength. The constant of proportionality depended on the baseline photocurrent ratio in the reference and signal channels, as derived in Eq. (4). This ratio varied considerably from day to day and setup to setup with changes in fiber alignment. Although absolute absorption measurements are possible if the baseline ratio is known, the results reported here were calibrated against known or estimated concentrations because the baseline ratios were not separately recorded. Figure 7 compares the water concentration measured in the combustion gases using the 7612 and 7605.8-cm^{-1} transitions to equilibrium predictions at the known stoichiometry and flame temperature. The measured data were calibrated against the equilibrium predictions at a single intermediate point corresponding to 9×10^{17} cm^{-3}. This constant calibration factor is applied to the remainder of the measured absorbances in order to place the data on a relative scale. The lowest concentration data points correspond to flame temperature below 1000 K, where both measurements indicate that the mixture stoichiometry is too low to achieve equilibrium at the measurement location 1 cm downstream of the burner surface. The typical error bars shown for these data indicate that the estimated potential deviations from equilibrium are much larger than the measurement uncertainty. The 7612-cm^{-1} transition is very weak at flame temperatures and the relatively low signal-to-noise data results in poorer agreement with equilibrium predictions compared to results based on the stronger 7605.8-cm^{-1} transition, although the scatter in the data is within the estimated measurement uncertainty. For the stronger 7605.8-cm^{-1} transition measurements, the high-temperature data agree with the equilibrium predictions to within an rms uncertainty of ±2.5% over the range.

Figure 8 is a comparison of the measured temperature from the absorbance ratio of the 7612/7605.8 and 7612/7600.13 pairs with thermocouple data over the range 300–1900 K, encompassing both cell and flame data. The absolute values of the absorbance ratio data sets for a given line pair were calibrated against the thermocouple data with a single calibration point giving the minimum

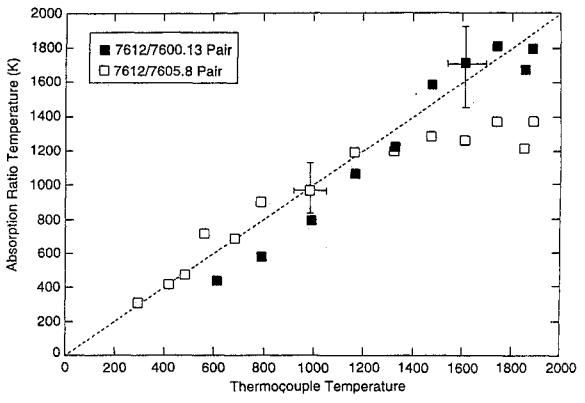

Fig. 8 Comparison of temperature measurements obtained with 7612/7605.8 line pair and 7612/7600.13 line pair to radiation-corrected thermocouple measurements.

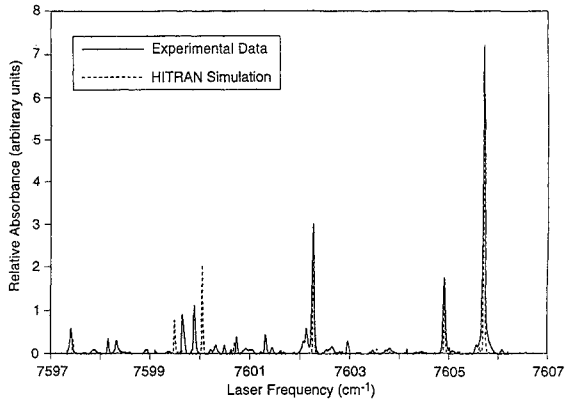

Fig. 9 Comparison of HITRAN simulation and experimental spectrum at 1200 K and 30 torr.

least-squares difference. The absolute values of the individual line strengths and their ratio could be determined if the baseline ratio signals are separately recorded. Further work is planned to determine these fundamental line strengths so as to eliminate the need for a thermocouple calibration.

For the 7612/7605.8 pair at temperatures between 300 and 1300 K, the data determined from the absorbance ratio agree with the thermocouple data with an rms standard deviation of 42 K over the range. Above 1300 K the measurement uncertainty of about 10% in the absorbance ratio corresponds to temperature uncertainties exceeding several hundred Kelvins, as predicted by the analysis summarized in Fig. 5. The data for this line pair above about 1300 K have essentially no temperature sensitivity. For the 7612/7600.13 pair, the overall agreement is somewhat poorer than with the 7612/7605.8 pair, principally due to the larger measurement uncertainty resulting from the lower absorbance on the 7600.13-cm^{-1} line, although temperature sensitivity is retained to higher temperatures, as predicted in Fig. 5. It is important to note in Fig. 8 that the error bars are representative of the uncertainty at the condition shown. In fact, the signal strengths and temperature sensitivity of the measured line strength ratio varies by orders of magnitude across this temperature range. Further work is required to develop a statistical analysis of multiple determinations over a period of several days with changing optical alignment.

In attempting to extend the 7612/7600 ratio data set to lower temperatures using the variable temperature cell, we discovered several inconsistencies between the experimental spectra and the HITRAN simulations used to reduce this data to temperature. Figure 9 shows a measured absorption spectrum obtained with the cell at 1200 K and 30 torr compared to a HITRAN simulation. The experimental spectrum was acquired by adjusting the diode laser temperature to a setpoint and ramping the injection current so as to scan the laser over a 2–2.5 cm^{-1} region, adjusting the temperature to a new value and repeating the process until five overlapping spectra

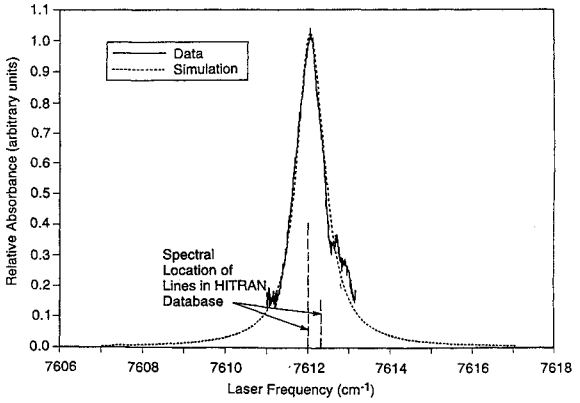

Fig. 10 Comparison of measured line shape fragment and calculated Voigt profiles for the blended features near 7612 cm^{-1} at 5.0 atm and 473 K.

had been obtained. The overlapping spectra were integrated into a single continuous spectrum and placed on an absolute frequency scale by matching the separation between the strong features at 7602.3 and 7605.8-cm^{-1}. The absolute value of HITRAN simulation was scaled to the peak of the 7605.8-cm^{-1} transition. Most of the major absorption features are predicted by the HITRAN model in the proper relative strength, with the pronounced exception of the 7600.13-cm^{-1} transition that we were attempting to use for thermometry. Clearly both the frequency and strength of this feature are not correctly predicted by HITRAN, and the blending of this feature with the neighboring transition near 7599.7-cm^{-1} renders this transition problematic at low temperatures. Also notable in the experimental spectrum are numerous weak transitions not included in the HITRAN simulation. These features presumably arise from higher energy level absorbing states that the HITRAN database does not include. It is likely that they represent superior choices for high-temperature thermometry and will be further explored in future work. These results indicate the need for basic spectroscopic data of high-temperature water vapor transitions in this wavelength region.

Work is also continuing to extend these techniques to higher pressures for sensor applications within an aeropropulsion system. Initial cell data at pressures up to 5.0 atm show that partially resolved transitions may be probed, although only about 80% of the room-temperature integrated line strength may be captured in a ~2-cm^{-1} scan. Figure 10 is an example of a partially resolved line shape obtained at 5 atm and 473 K. The experimental data are plotted against a calculated profile consisting of the two merged transitions near 7612 cm^{-1} and illustrate that although the laser scan was over 2 cm^{-1}, only a portion of the collision-broadened line was captured. The experimental data also indicate that the two transitions are less blended than is predicted by HITRAN broadening data. Ratiometric temperature measurements are further complicated by contributions from the Lorenztian wings of neighboring transitions, resulting in a complex temperature dependence. Techniques are being developed to explore the feasibility of quantitative ratiometric thermometry at elevated pressures using partially resolved transitions and detailed spectral modeling.

V. Summary and Conclusions

This paper reports results on the progress of development of aeropropulsion sensors based on near-IR diode laser absorption. Using a balanced ratiometric detection technique, a compact sensor architecture is demonstrated that allows sensitive measurements of aerodynamic and combustion species without resort to frequency/wavelength modulation techniques or custom-fabricated lasers operating at specially chosen wavelengths. Using widely available, broadly tunable InGaAsP diode lasers near 1.31 μm, simultaneous water density and temperature measurements are demonstrated with limiting density sensitivity of 10^{15} cm^{-3} in a 50-cm path and an rms standard deviation of 42 K over a range from 300 to 1300 K. Initial results suggest the possibility of extending this temperature range to 1900 K and above using other line pairs.

Initial results at 5.0 atm are presented that imply detailed spectral modeling will be required to interpret partially resolved spectral at high pressure.

Acknowledgments

Portions of this work are supported by the NASA Dryden Flight Research Facility, the NASA Langley Research Center, and the Air Force Wright Laboratory. The authors acknowledge the assistance of Dan Palombo in the balanced ratiometric circuit design and analysis and the helpful comments and guidance of Steven Davis.

References

[1]Phillipe, L. C., and Hanson, R. K., "Laser Diode Wavelength-Modulation Spectroscopy for Simultaneous Measurement of Temperature, Pressure, and Velocity in Shock-Heated Oxygen Flows," *Applied Optics*, Vol. 32, No. 30, 1993, pp. 6090–6103.

[2]Arroyo, M. P., and Hanson, R. K., "Absorption Measurements of Water-Vapor Concentration, Temperature, and Line-Shape Parameters Using a Tunable InGaAsP Diode Laser," *Applied Optics*, Vol. 32, No. 30, 1993, pp. 6104–6116.

[3]Arroyo, M. P., Langlois, S., and Hanson, R. K., "Diode-Laser Absorption Technique for Simultaneous Measurements of Multiple Gasdynamic Parameters in High-Speed Flows Containing Water Vapor," *Applied Optics*, Vol. 33, No. 15, 1994, pp. 3296–3307.

[4]Arroyo, M. P., Birbeck, T. P., Baer, D. S., and Hanson, R. K., "Dual Diode-Laser Fiber-Optic Diagnostic for Water-Vapor Measurements," *Optics Letters*, Vol. 19, No. 14, 1994, pp. 1091–1093.

[5]Baer, D. S., Hanson, R. K., Newfield, M. E., and Gopaul, N. K. J. M., "Multiplexed Diode-Laser Sensor System for Simultaneous H_2O, O_2, and Temperature Measurements, *Optics Letters*, Vol. 19, No. 22, 1994, pp. 1900–1902.

[6]Allen, M. G., Carleton, K. L., and Davis, S. J., "Ultrasensitive Diode Laser Direct Absorption Measurements: Applications to Mass Flux Flight Instrumentation," *Laser Applications in Combustion and Combustion Diagnostics II*, Vol. 2122, Society of Photo-Optical Instrumentation Engineers, 1994, pp. 1–12.

[7]Allen, M. G., Carleton, K. L., Davis, S. J., and McManus, K. R., "Diode Laser-Based Measurements of Water Vapor and Ground State Oxygen in Chemical Oxygen Iodine Lasers," AIAA Paper 94-2433, June 1994.

[8]Allen, M. G., Carleton, K. L., Davis, S. J., Kessler, W. J., Otis, C. E., Palombo, D. A., and Sonnenfroh, D. M., "Ultra-Sensitive Dual-Beam Absorption and Gain Spectroscopy: Applications for Near-IR and Visible Diode Laser Sensors," *Applied Optics*, Vol. 34, No. 18, 1995, pp. 3240–3249.

[9]Bomse, D. S., Stanton, A. C., and Silver, J. A., "Frequency Modulation and Wavelength Modulation Spectroscopies: Comparison of Experimental Methods Using a Lead-Salt Diode Laser," *Applied Optics*, Vol. 31, No. 6, 1992, pp. 718–731.

[10]Phillipe, L. C., and Hanson, R. K., "Tunable Diode Laser Absorption Sensor for Temperature and Velocity Measurements of O_2 in Air Flows," AIAA Paper 91-0360, Jan. 1991.

[11]Langlois, S., Birbeck, T. P., and Hanson, R. K., "Diode Laser Measurements of H_2O Line Intensities and Self-Broadening Coefficients in the 1.4 μm Region," *Journal of Molecular Spectroscopy*, Vol. 163, 1994, pp. 27–42.

[12]Hobbs, P. C. D., "Shot Noise Limited Optical Measurements at Baseband with Noisy Lasers," *Laser Noise*, Vol. 1376, Society of Photo-Optical Instrumentation Engineers, 1990, pp. 216–221.

[13]Haller, K. L., and Hobbs, P. C. D., "Double Beam Laser Absorption Spectroscopy: Shot Noise-Limited Performance at Baseband with a Novel Electronic Noise Canceler," *Optical Methods for Ultrasensitive Detection and Analysis: Techniques and Applications*, Vol. 1435, Society of Photo-Optical Instrumentation Engineers, 1991, p. 298.

[14]Houser, G. D., and Garmire, E., "Balanced Detection Technique to Measure Small Changes in Transmission," *Applied Optics*, Vol. 33, No. 6, 1994, pp. 1059–1062.

[15]Rothman, L. S., et al., "The HITRAN Database: 1986 Edition," *Applied Optics*, Vol. 26, No. 19, 1987, pp. 4058–4097.

[16]Toth, R. D., "Extensive Measurements of $H_2{}^{16}O$ Line Frequencies and Strengths: 5750 to 7965 cm^{-1}," *Applied Optics*, Vol. 33, No. 21, 1994, pp. 4851–4867.